J. Water Environ. Nanotechnol., 3(3): 219-234 Summer 2018

ORIGINAL RESEARCH PAPER

Fabrication, Characterization, Regeneration and Application of Nanomagnetic Fe_3O_4@Fish Scale as a Bio-adsorbent for Removal of Methylene Blue

Nima Gholami Ahmadgurabi[1], Ahmad Dadvand Koohi[1]*, Azadeh Ebrahimian Pirbazari[2]

[1] Chemical Engineering Department, Engineering Faculty, University of Guilan, Rasht, Iran
[2] Fouman Faculty of Engineering, College of Engineering, University of Tehran, Fouman, Iran

Received: 2018.04.28 Accepted: 2018.06.22 Published: 2018.07.30

ABSTRACT

The methylene blue (MB) adsorption from aqueous solution was investigated through Fe_3O_4 nanoparticles loaded on Fish Scale (FS) from fishery biomass. The presence of collagen fibers, apatite crystals and nano-magnetite particles in the structure of nano-magnetic fish scale (MFS) was observed in FTIR, EMA and XRD results. From nitrogen physisorption studies, the FS and MFS specific surface areas were estimated at 0.65 and 4.86 m^2/g, respectively. The negative values of ΔG^0 and ΔH^0 confirmed that the adsorption was a spontaneous and exothermic process, respectively. The MB adsorption onto MFS was a physisorption controlled process. The Sips equation estimated the best fit to the data compared with other isotherm equations. The Langmuir and Sips maximum adsorption capacities (Q_{max}) were 68.72 and 60.87 mg/g, respectively. MB removal by MFS followed the model of pseudo-second order rate kinetics. The reusability potential of the MFS was studied, and results showed an efficiency of 59.63%.

Keywords: *Adsorption, Fish Scale, Methylene Blue, Nanomagnetic, Regeneration*

How to cite this article
Gholami Ahmadgurabi N, Dadvand Koohi A, Ebrahimian Pirbazari A. Fabrication, Characterization, Regeneration and Application of Nanomagnetic Fe_3O_4@Fish Scale as a Bio-adsorbent for Removal of Methylene Blue. J. Water Environ. Nanotechnol., 2018; 3(3): 219-234. DOI: 10.22090/jwent.2018.03.003

INTRODUCTION

Nowadays, there is no way for development without environmental considerations. Dyes are of primary concerns in the environment pollution because they hinder aquatic plants photosynthesis. Everyday considerable amount of colored wastewater is released from the industries including leather, paper, textile, pulp, tannery, and paint (Rafatullah *et al.*, 2010). Since dye pollution can be toxic and may affect both humans' and plants' health, the governmental legislation in many countries require regulations for the treatment of dye effluents before discharging to the environment (Rafatullah *et al.*, 2010; Salleh *et al.*, 2011). Different methods can remove dyes such as chemical oxidation [1], membrane separation [2], photocatalytic and electrochemical degradation [3], and adsorption [4]. Among these, adsorption is one of the most economical and efficient methods [5,6]. Low-cost and efficient adsorbents should be developed to eliminate dyes from wastewater. In recent years, low-cost adsorbents, specially adsorbents loaded with Fe_3O_4 nanoparticles, has made many scholars to develop new effective low-cost environmentally friendly adsorbents such as wheat straw, rice straw, peanut hull, walnut sawdust and banana peel [5,7,8]. The selection of adsorbent depends on its performance, availability, and cost. The involvement of magnetic nanoparticles in the structure of bioactive adsorbents has solved the problem of separating adsorbents from aqueous ambiance which can cause secondary pollution of the aqueous medium through a magnetic

* Corresponding Author Email: *dadvand@guilan.ac.ir*

field. Some specifications of these nanoparticles including ease of synthesis, cost-effective, easy manipulation via functionalization and coating, easy recovery, absence of secondary contamination and environmental friendliness has been considered with many researchers as well as the use of these nanoparticles in the structure of adsorbents due to the high surface area of magnetic nanoparticles [9,10]. FS represents a highly accessible residue in the industry of fisheries [11]. Disposal of waste from the fishing industry can cause environmental problems. Therefore, it is very important to make use of the benefits of the waste. It is reported that Fish scales consist of collagen fibers which are surrounded by calcium and hydroxyapatite [12]. Presence of functional groups including amide and carboxyl in the fish scale structure can cause adsorption of toxic substances using electrostatic attraction [12]. In another hand, the porous structure of hydroxyapatite has good adsorption abilities. Even though FS has been used in many articles as a source of minerals such as hydroxyapatite [13] and collagen [14,15], there is just a few research on evaluating its potential as an adsorbent, like adsorption of reactive blue 5G [11], Pb^{2+} [16], dichlorophenol-2,6-indophenol and Ponceau 4R [12]. Ribeiro *et al.* [11] showed that untreated and acid treated fish scales can be used for removal of reactive blue 5G as an anionic dye from aqueous solution with a maximum adsorption capacity of 241.2 mg/g at pH = 2.

In all previous studies, a roughly similar method has been used for the application of FS (without modification). A nano-magnetic adsorbent was produced by modifying the surface of common carp FS with Fe_3O_4 nanoparticles in order to assess its capacity as an adsorbent to remove MB dye in a batch system. This is the first research on adsorption of a cationic dye by an FS based adsorbent modified by Fe_3O_4 nanoparticles. First, the structure and morphology of the magnetic FS were specified using Fourier transform infrared spectroscopy (FTIR), nitrogen physisorption and field emission scanning electron microscopy (FESEM). Then, all controlling factors and conditions of optimization was explored and evaluated which are reaction contact time, initial dye concentration, pH, and the regeneration efficiency of the magnetic adsorbent.

EXPERIMENTAL SECTION

Materials

The FSs were obtained from the fish bazaar in Rasht, Guilan Province, Iran. Common carp was chosen among the many kinds of fishes used in the north of Iran because of its abundance and favorable scale size. MB was purchased from Merck ($C_{16}H_{18}N_3SC$, M=319.8 g/mol, density=1.757 g/mL), and chosen as a representative reactive dye. An MB stock solution was provided via dissolving 1.0g of MB in distilled water (1 L), and the different MB solutions (50–500 mg/L) were obtained by diluting the stock solution. The solution pH was set to the desired value via adding 0.1 M and/or 0.01 M of HCl or NaOH. $FeSO_4.7H_2O$ (M=278.02 g/mol, density=1.895 g/mL) and $FeCl_3.6H_2O$ (M=270.33 g/mol, density=1.82 g/mL) were purchased from Ghatran Shimi Co., Iran.

Preparation of Initial Adsorbent

Initially, the FSs were entirely rinsed with tap water, and then they were washed with sodium hypochlorite solution (5% wt) to eliminate any adhering dirt; simultaneously they were deodorized and degreased. Finally, the raw materials were rinsed with distilled water and were dried at 80 °C for 24 h. Finally, the FSs were crushed, sieved into 100–500 µm size range, and preserved in desiccators (Fig. 1a).

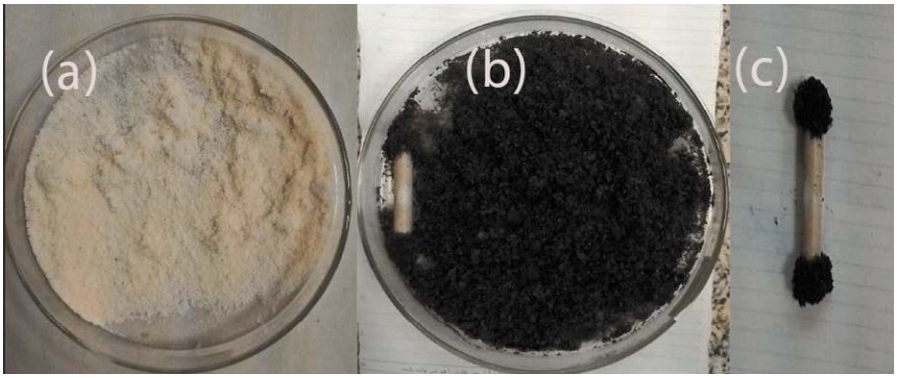

Fig. 1. Photograph of (a) powdered Fish scale and (b) Fish scale after impregnation of Fe_3O_4 nanoparticles (c) Magnetic fish scale attached to a magnetic rod.

Synthesis of Nano-Magnetic FS

The technique of chemical precipitation was applied to provide particles which have a narrow size distribution and homogeneous composition. 3.2 g of $FeSO_4.7H_2O$ and 6.2 g of $FeCl_3.6H_2O$ (Fe (III): Fe (II) molar ratio was 2:1) were dissolved in 160 mL of distilled water with severe stirring and an inert atmosphere to obtain 4 g of magnetic particles, 20 mL of ammonium hydroxide solution (25 %) was added while the solution was getting heated to 80 °C. Next, as the solution color varied from light brown to black, the solution was left for 10 min to make sure about the ultimate growth of the crystals of the nanoparticle. Afterward, 20 g of pulverized FS was added to the solution, and the reaction was being done for 70 min at 80±1 °C with continuous stirring. Finally, the suspension was cooled to room temperature, and then it was washed several times using distilled water to eliminate chemicals which were un-reacted. Magnetic nanoparticles of Fe_3O_4–fish scale (MFS) adsorbents were tested with a magnetic rod, and the synthesized adsorbents (MFS) were attracted to the magnetic rod, which could be due to the iron's magnetic behavior (Fig. 1b,c). The reactions occurring in MFS generation are shown as follows:

$$2FeCl_3.6H_2O + FeSO_4.7H_2O + 8NH_4OH \rightarrow 6NH_4Cl + (NH_4)_2SO_4 + Fe_3O_4 + 17H_2O \quad (1)$$

$$FS + Fe_3O_4 + H_2O \rightarrow MFS \quad (2)$$

Characterization Instruments

FTIR (Bruker, USA, Alpha) of the dried MFS, before and after MB adsorption, was done in the wavenumber range of 400-4000 cm^{-1} for determination of the binding groups' type on the adsorbent by employing KBR pallet pressed disk technique. The area of the specific surface on the basis of nitrogen physisorption was estimated by the Brunauer–Emmett–Teller (BET) theory. The morphology and surface structure of FS and MFS were specified by utilizing FESEM at a 20 kV acceleration voltage before and after MB adsorption (FESEM, TESCAN-VEGA, Czech Republic). The overall chemical composition was determined by an EDX spectrometer (Oxford instruments-INCA, England) coupled to the FESEM. Elemental distribution spectroscopy (EDS) and elemental distribution mapping (EDM) analysis were also performed. The adsorbents' XRD patterns were achieved by a diffractometer (SIEMENS, D5000, GERMANY, λ=1.54059) with Cu anode and linear focus (40mA and 40kV) in steps of 0.03° from 2θ=10° to 70° for studying the nature of adsorbents.

Point of Zero Charge (pH_{pzc})

The point of zero charges (pH_{pzc}) was specified by using 0.01 M NaCl solution. First, the NaCl solutions' pH was set at 3-11 via adding adequate ate value of 0.01 M and/or 0.1 M NaOH or HCl solution. Second, 0.1 g of adsorbent was added to the solutions; then, the solutions' final pH was obtained after 48 h. The pH_{pzc} was obtained from the intersection point of the curve of pH_{final} vs. $pH_{initial}$.

Batch adsorption experiments

In order to determine the effect of contact time and the equilibrium time, batch kinetic experiments were done by adding a fixed amount of FS and MFS (0.3 g) into 50 mL of the MB solution at constant initial concentration (200 mg/L) at 303K and pH of 8 and shaking for predetermined intervals of time (up to 160 min). The each MB solution concentration at different time intervals was determined by using a UV–vis spectrophotometer (Rayleigh UV-2601, China). Also, optimum adsorbent dosage was determined with adding different amounts of MFS (0.05–0.5 g) into the 50 mL MB solution (200 mg/L) with a constant pH of 8 at 303K.

Equilibrium and Kinetic Studies

The effect of MB solution initial pH on adsorption of MB was assessed by dissolving 0.3 g of MFS to the MB solutions (50mL-100 mg/L) with various initial pHs of 3.3, 5.2, 7, 8.9, and 10.9 at 303 K. Equilibrium evaluations were done through adding a constant value of MFS (0.3 g) with 50 mL of the MB solutions by various initial concentrations (50, 100, 200, 300, 400, and 500 mg/L) at 303, 313 and 323 K and pH of 8. The concentration of MB solutions was indicated using spectrophotometry at the peak absorbance wavelength (665 nm) by a double beam UV–vis spectrophotometer. Adsorption kinetics experiments were done via dissolving 100 mL of the MB solution with various initial concentrations (50, 100 and 200 mg/L) with 0.6 g of MFS at room temperature. The MFS equilibrium adsorption capacity was calculated as follows [4].

$$q_e = \frac{C_0 - C_e}{M} V \quad (3)$$

Where q_e is the dye amount taken up by the adsorbent (mg/g) at equilibrium; C_0 is the initial concentration of dye (mg/L); C_e is the equilibrium concentration of dye (mg/L). V is the dye solution volume (L), and M is the adsorbent's mass (g).

Adsorption Isotherm and Kinetic Models

The data of equilibrium isotherm were consistent with some popular nonlinear two /three parameters- isotherm models included Langmuir, Freundlich, Sips, and Redlich-Peterson by using the curve fitting toolbox of MATLAB software (R2014a). The Langmuir isotherm can be expressed as follows [17]:

$$q_e = Q_{max} K_L C_e / (1 + K_L C_e) \quad (4)$$

Where q_e *(mg/g)* is the adsorbed amount of dye, Q_{max} *(mg/g)* is the Langmuir maximum adsorption capacity, K_L *(L/mg)* is the Langmuir adsorption constant, and C_e *(mg/L)* is the equilibrium concentration of the dye in solution. The Freundlich isotherm can be expressed as follows [17]:

$$q_e = K_F C_e^{1/n} \quad (5)$$

Where K_F $(mgg^{-1}(mgL^{-1})^{-1/n})$ and n are fitting constants which can be related to capacity and strength of adsorption, respectively. The Sips and Redlich-Peterson three-parameter isotherms can be written in the following forms, respectively:

$$q_e = Q_{max} K_s C_e^{1/n} / (1 + K_s C_e^{1/n}) \quad (6)$$

$$q_e = K_{RP} C_e / (1 + \alpha C_e^{\beta}) \quad (7)$$

Where K_s $((mg^{-1})^{-1/n})$ and n are fitting constants of Sips isotherm, K_{RP} (Lkg^{-1}) and α $(kgmg^{-1})$ are fitting constants of Redlich-Peterson, and β is basically in the range of zero to one. The appropriateness of these models was assessed using a non-linear correlation coefficient (R^2) [18].

The dynamics of MB adsorption was studied using the linear form of pseudo-first-order and the pseudo-second-order models, which were represented by the following equations, respectively [5,19]:

$$\ln(q_e - q_t) = \ln q_e - k_1 t \quad (8)$$

$$t/q_t = 1/k_2 q_e^2 + t/q_e \quad (9)$$

q_e and q_t are the adsorption capacities of MFS (mg/g) at equilibrium and any instant of time, respectively. k_1 and k_2 (1/min) are the rate constant of pseudo-first order and pseudo-second order (g/mg.min), respectively. The plots' slope and intercept between $ln(q_e-q_t)$ vs. t and t/q_t vs. t give the values of k_1 and k_2, respectively.

Regeneration Study

5g of used-MFS (UMFS) was initially washed with tap water and then treated with HCl (0.1 N, 500 mL) for 24 h to study the reusability capacity of the UMFS. Finally, it was extensively washed using distilled water several times so that neutral pH was obtained. Since desorption of MB is favorable at low pH values, HCl can be appropriate for regeneration purpose. The regenerated MFS (RMFS) was dried and stored for further experiments. The equilibrium studies were conducted with the same conditions of main experiments (MFS adsorbent experiments) at 303 K.

RESULTS AND DISCUSSION

Characterization

FTIR Analysis

The MFS's and UMFS's FTIR spectra are depicted in Fig. 2a and b. In summary, the FTIR absorption bands of PO_4^{3-} (1038 cm^{-1}) (Nadeem *et al.*, 2008)and CO_3^{2} (875, 1448, and 1544 cm^{-1}) [16,20] can be associated with hydroxyapatite and carbonated apatite in FS, respectively (Fig. 2a). Generally, FSs are composed of hydroxyapatite and collagen [21]. The presence of collagen in the structure of adsorbent can be approved by five main bands of absorption at 1544 cm^{-1} (amide II), 1239 cm^{-1} (amide III), 1639 cm^{-1} (amide I), 3419 cm^{-1} (amide A), and 2930 cm^{-1} (amide B) [15]. The peak at 605 cm^{-1}can be due to the presence of Fe–O group, which is related to the Fe_3O_4 nanoparticles on the adsorbent [22]. The peak at 3419cm^{-1} was assigned to water (H_2O), and a small band at 2364 cm^{-1} was attributed to potassium bromide (KBr), which can be related to KBr pressed disk method of FTIR [23], which was mentioned in characterization instruments section. The FTIR spectrum of UMFS in Fig. 2b shows that after MB adsorption, some structures such as collagen (1239 cm^{-1}), hydroxyapatite (1038 cm^{-1}) and carbonated apatite (1544 cm^{-1}) have been weakened or removed from the adsorbent, which can be due to an adsorbate-adsorbent interaction in the MB solution.

Nitrogen Physisorption (BET Isotherm)

Based on the BET isotherm, the FS's and MFS's

specific surface areas were obtained at 0.65 and 4.86 m^2/g, respectively. The surface area of the magnetic adsorbent (MFS) was more than seven times greater than before the loading of nanomagnetic particles (FS) on it. However, Ribeiro *et al* [11], and Ho *et al*. [24] reported the specific surface area (BET method) of Oreochromis niloticus and Malaysia local fishes equal to 2.6 and 0.15 m^2/g, respectively. It is clear that loading of Fe_3O_4 nanoparticles on FS has a great impact on the improvement of its specific surface area.

ESEM Analysis

The FESEM micrographs of FS, MFS, and UMFS are shown in Fig. 3 with double magnifications. The surface of FS was found to be homogeneous with tiny cracks (Fig. 3a and a´), by which it's non-porous morphology was confirmed, and also has identical and arranged growth rings which were distributed on the adsorbent surface [11]. Therefore, FS is solid along with a rare value of mesopores which tends to be a non-porous adsorbent. However, after the loading of Fe_3O_4 nanoparticles on FS, the surface

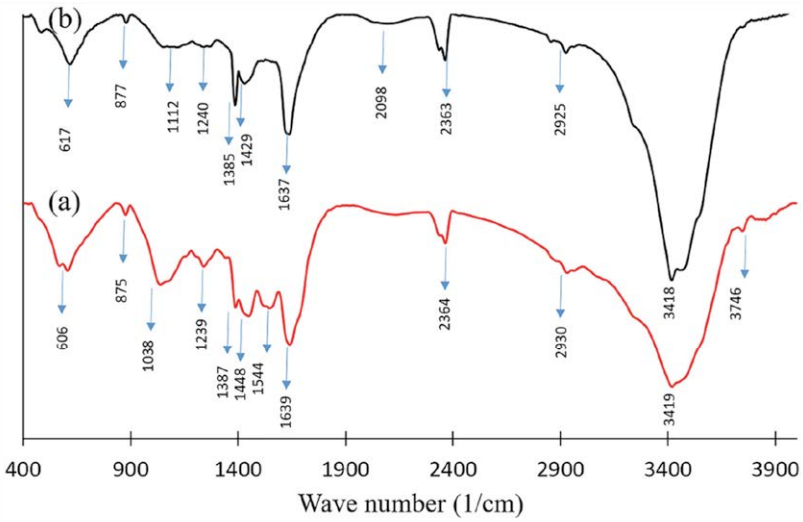

Fig. 2. FTIR spectra of the adsorbent (a) before (MFS) and (b) after (UMFS) adsorption of MB.

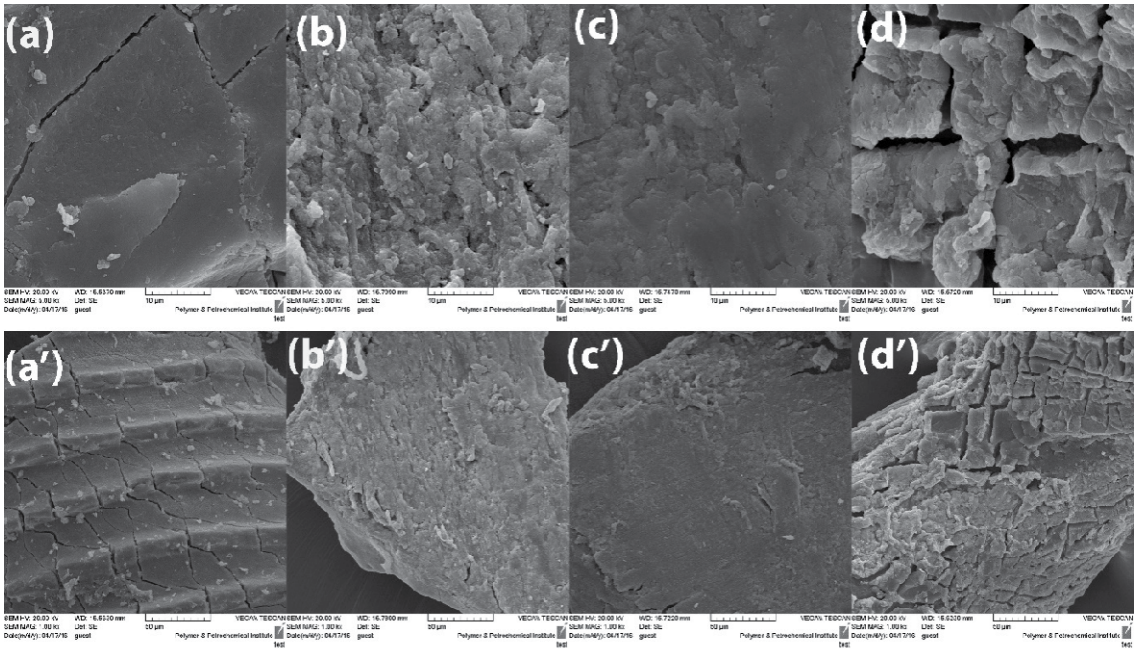

Fig. 3. FESEM images of (a) FS scale:10μm, (a´) FS scale: 50 μm, (b) MFS scale: 10μm, (b´) MFS scale: 50μm, (c) UMFS scale: 10μm, (c´) UMFS scale: 50μm, (d) RMFS scale: 10μm, and (d´) RMFS scale: 50μm.

of adsorbent showed heterogeneous and porous structure (Fig. 3b and b´). Different morphological patterns become clear by comparing Fig. 3a and b. Some of the Fe_3O_4 nanoparticles are shown by crystal diameter with yellow lines in the Fig. 4. Since the crystal diameters are less than 100nm, it can be approved that Fe_3O_4 nanoparticles have been successfully synthesized on FS. A complete surface coverage of adsorbent by MB is shown in Fig. 3c and c´. The surface of the adsorbent was homogenized, smoothed and less porous after adsorption of MB. The FESEM images after the regeneration process are shown in Fig. 3d and d´. It can be seen that the uniform layer of dye molecules on UMFS has mostly been cleared from the adsorbent surface, and the initial adsorbent's mesoporous structure became apparent.

EDX, EDS and (EMA)

The overall elemental chemical analysis of FS, MFS, and UMFS was identified and qualified using EDX (Table 1) and EDS (Fig. 5). The existence and the atomic percent of the elements, which are reported in Table 1 and Fig. 5, respectively, can render a superior perception of the adsorption process. Some of the most important ones are discussed below:

a) Cl element: Presence of Cl element may be related to the pretreatment of FS by sodium hypochlorite, which is mentioned in the preparation of initial adsorbent section. The slight atomic percent of Cl reported in Table 1 can confirm the latter conclusion. The atomic percent of Cl decreased in MFS and UMFS because of Fe_3O_4 loading and adsorption of MB, respectively. The

Table 1. Chemical composition based on the atomic percent obtained by EDX analysis

Elements (%)	FS	MFS	UMFS	RMFS
C	27.32	26.64	23.47	52.45
N	-	-	14.75	-
O	49.03	52.63	49.08	38.81
Na	0.51	0.56	0.94	-
Mg	0.52	0.25	0.40	-
P	9.04	2.91	3.27	0.08
S	-	-	0.12	-
Cl	0.10	0.06	0.03	0.26
Ca	13.48	5.18	4.57	0.05
Fe	-	11.77	3.37	8.85

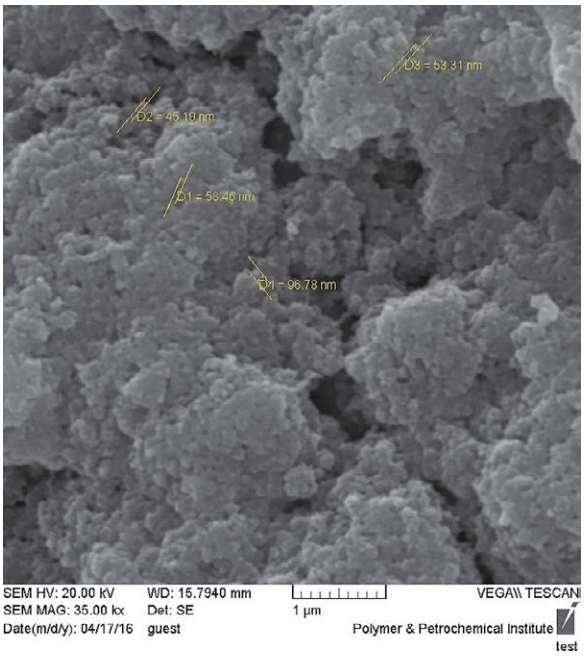

Fig. 4. Particle diameters of Fe_3O_4 nanoparticles in FESEM image of MFS.

reason for the increase in the atomic percent of Cl in the regenerated adsorbent (RMFS) will be explained in the regeneration section.

b) Fe element: As it is obtained from Table 1 and Fig. 5, there is no Fe element on FS before modification by Fe_3O_4 nanoparticles and, as a result, the presence of Fe in MFS can approve the loading of Fe_3O_4 nanoparticles onto FS. The atomic percent of Fe decreased in UMFS because of the adsorption of MB. The reason for the increase in the atomic percent of Fe in RMFS will be explained in the regeneration section. The EMA analysis of Fe element on the surface of MFS is shown in Fig. 6a, where red points represent the Fe element.

c) N and S elements: The FS composition mainly includes C, O, P and Ca elements [11]. It initially does not have any N or S element (Table 1). Since N and S elements are included in the structure of MB molecule ($C_{16}H_{18}N_3SC$), the presence of N or S element in the composition of UMFS (Table 1 and Fig. 5c) can confirm the adsorption of MB on FS. The EMA analysis of N element on the surface of UMFS is shown in Fig. 6b, where red points represent the N element.

XRD Analysis

The patterns of XRD of FS and MFS powders are displayed in Fig. 7. The diffraction peaks for FS are

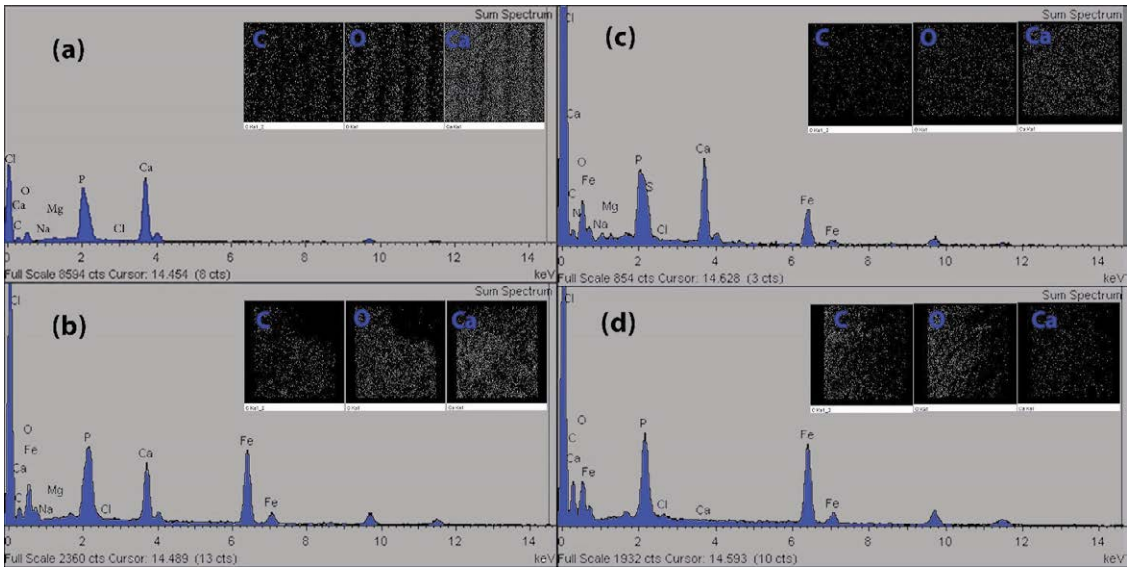

Fig. 5. EDS analysis of (a) FS, (b) MFS, (c) UMFS and (d) RMFS.

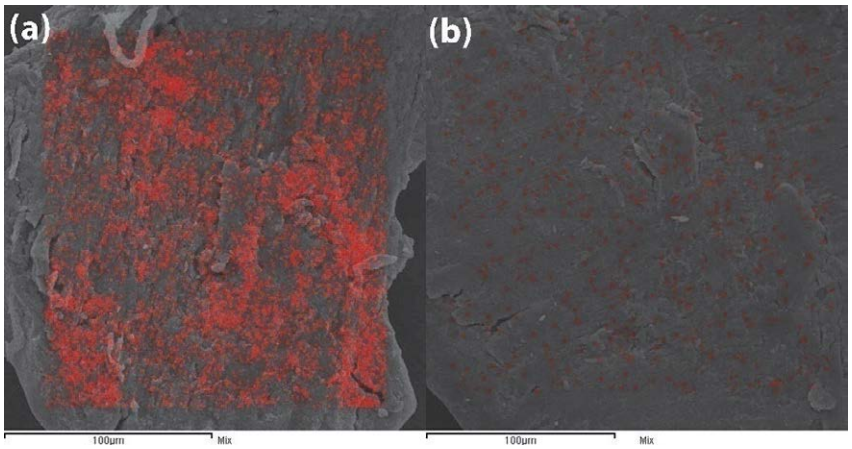

Fig. 6. The EMA analysis of (a) Fe element on the surface of MFS, and (b) N element on the surface of UMFS.

at 2θ = 26°, 32°, 40°, 47°, 49.5°, 54° and 64° (Fig. 7a). As previously mentioned, FS mainly consists of hydroxyapatite; therefore, this peaks' composition is in agreement with the powder of hydroxyapatite from crystallography open database [24]. According to the XRD pattern of synthesized Fe_3O_4 (data not shown), the diffraction peaks for Fe_3O_4 crystals are at 2θ=30.2°, 35.6°, 43.5°, 54.3°, 57.4° and 63.1° [25]. Consequently, loading of Fe_3O_4 nanoparticles on FSs can be approved by the presence of three peaks, which are shown with black circles on the XRD pattern of MFS (Fig. 7b), but not on the XRD pattern of FS. The broad crystalline diffraction around 2θ=20° represents the amorphous structure of the collagen [26].

Operating Parameters

Determination of the pH of Point of Zero Charge (pH_{pzc}) and the Effect of the Initial pH of Solution

An influential factor of pH-sensitive adsorbents is pH_{pzc}, which specifies the linearity of pH sensitivity domain and then determines the surfaces' adsorption capabilities and the type of surface active centers. At pH_{pzc} the total surface positive charge is in equilibrium with the overall negative charge of the surface. Also, the surface is charged positively below pH_{pzc}, while at pH values above pH_{pzc}, the surface is charged negatively [23]. Adsorption of Cationic dye is desired at $pH > pH_{pzc}$ because of functional groups including groups of hydroxyl and carboxyl; and conversely, at $pH < pH_{pzc}$, adsorption of anionic dye is favored while the adsorbent surface becomes charged positively [9]. The pH_{final} versus pH_{initia} graph was drawn (Fig. 8a). The curves' intersection with the straight line for pH_{final} vs. pH_{initia} gives the pH_{pzc}, and the amount is 7.2 for MFS. Fig. 8b also presents the influence of initial pH of MB solution on the removal of MB. Fig. 8b shows that the MB removal percent rises with pH increasing. As the solution pH increases from 3.3 to 10.9, the removal percent improves from 75.34 to 98.96%. Accordingly, the solution's pH can be set to any value between 7.2 and 10.9. Even though the adsorption of MB increases with increasing the MB solution's initial pH, all experiments were conducted at pH of 8 because the MB solution's initial pH is about 5, and it is desirable to work as close as possible to neutral pH (acceptable pH limits (6.5-8.5) for releasing to the environment based on the Environmental Protection Agency (EPA)) as well as having an acceptable dye removal percent.

Generally, the functional groups of the adsorbent are affected by the solution's pH, and hence, it influences the adsorption process [23]. With considering the identified functional groups of MFS (amide, hydroxyapatite and carbonated apatite), the adsorption of MB onto MFS can take place through electrostatic interactions (between amide groups and MB dye functional groups) and

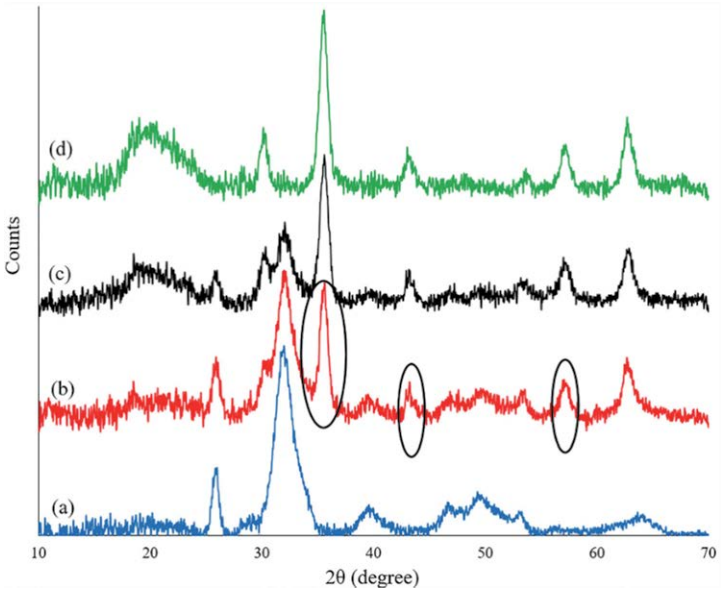

Fig. 7. XRD patterns of adsorbent (a) FS, (b) after nanoparticle impregnation (MFS), (c) after the adsorption of MB (UMFS), (d) after the regeneration process (RMFS).

H-bonding at pH=8. Based on pH_{pzc} analysis at $pH_{initial}>pH_{pzc}$ (pH_{pzc}=7.2), a slow rise in the MFS surface's negative charge density develops via increasing the pH of the solution. Therefore, in conditions of alkaline ($pH_{initial}>7$), an intensive electrostatic effect will occur between the MFS adsorbent and MB dye; however, at the initial $pH<pH_{pzc}$, an adverse electrostatic interaction will take place among the MFS surface, which is positively charged, and the cationic MB molecules through non-electrostatic mechanisms like van der Waals, H-bonding, and hydrophobic-hydrophobic interactions can occur [27]. Collagen is a triple helix with abundant amine and carboxylic acid functional groups. These functional groups in basic media are present predominantly in the $-COO^-$ and NH_2 form and therefore, the electrostatic interaction was taken place between the positive site of MB and mentioned ligands. Also, hydroxyapatite and magnetite exhibit amphoteric properties; therefore, in basic pH media, the MB dye adsorption onto MFS may be described from progress via the electrostatic attraction among negatively charged groups ($\equiv OPO_3H^-$ *and* FeO^-) of the MFS surface and positively charged groups (S^+) of the MB. The findings signify that the electrostatic interactions (COO/S^+, $N\text{-}H/S^+$, $apatite/S^+$,FeO^-/S^+) mainly account for the adsorption of MB dye onto MFS. A schematic of MB dye adsorption onto MFS is depicted in Fig. 8c.

Effect of contact time

It is important to determine the time to reach the equilibrium in the adsorption tests so that it can show how changes in the adsorption process are with time as well as the process controller stage. The adsorption capacity change with time is showed in Fig. 9. By considering the impact of contact time, the adsorption capacity increased with increasing the contact time up to 60 min for both FS and MFS and then remained almost stable with further increment in time up to 160 min. It seems that the process of adsorption is a

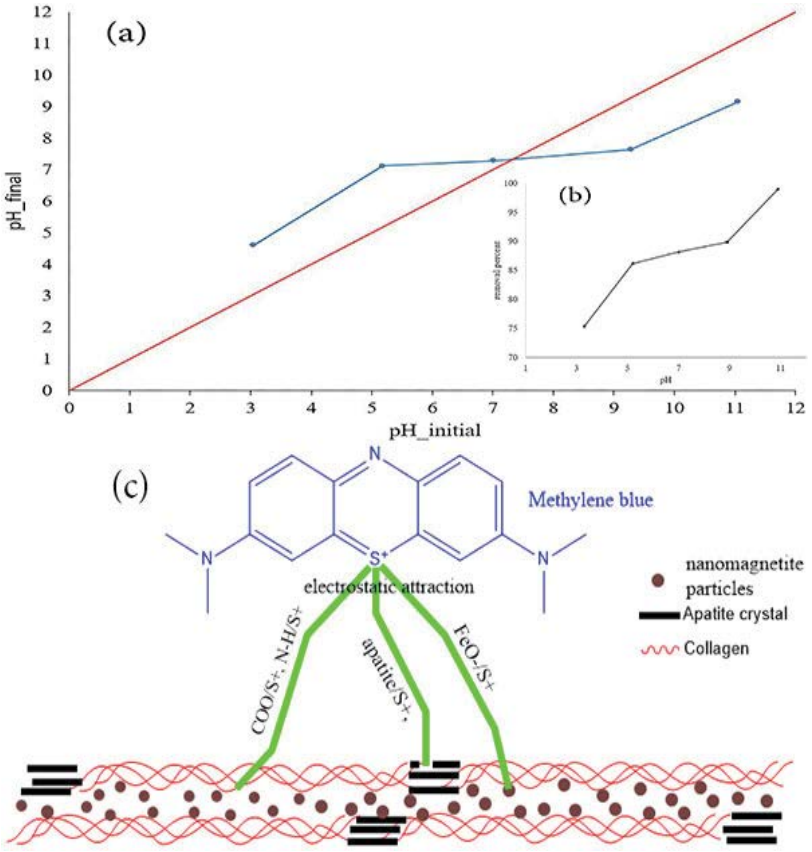

Fig. 8. (a) Plot for determination of pH_{pzc} for MFS, (b) Effect of the initial pH of MB solution onto the removal of MB and (c) Schematic diagram of MB dye adsorption onto MFS.

quick dye uptake in short periods of contact time. The reason for this phenomenon can be due to the fact that there are a large number of unoccupied active sites and functional groups were available for adsorption in the initial stage compared to that in the later stages [9,11]. Therefore, 60 min was designated as the optimum contact time for the adsorption of MB onto the MFS under our experimental conditions. Also, by comparing the absorption capacity of FS and MFs, it can be understood that the adsorption capacity of the MFS is 32% higher than that of the FS. This could be due to the modification of FS with Fe_3O_4 nanoparticles. So, MFS was used to continue the experiments.

Effect of adsorbent dosage

The variation of MB removal and adsorption values with MFS dosage are shown in Fig. 10. The amounts of adsorbed MB per unit mass of adsorbent reduced from 66.7 to 9 mg/g with the increase in adsorption dosage from 0.05 to 0.5 g. the results show that the removal percentage increased from 66.7 to 90%, by increasing the adsorbent amount from 0.05 to 0.3 g and then reach a plateau. This can be explained by the following reasons: 1) it can be relevant to aggregation/agglomeration of adsorbent particles at higher concentrations, thereby lead to a decline in the surface area of adsorbent and also an increase in the diffusion path length [4]. 2) Also, it can be related to the binding of almost all MB

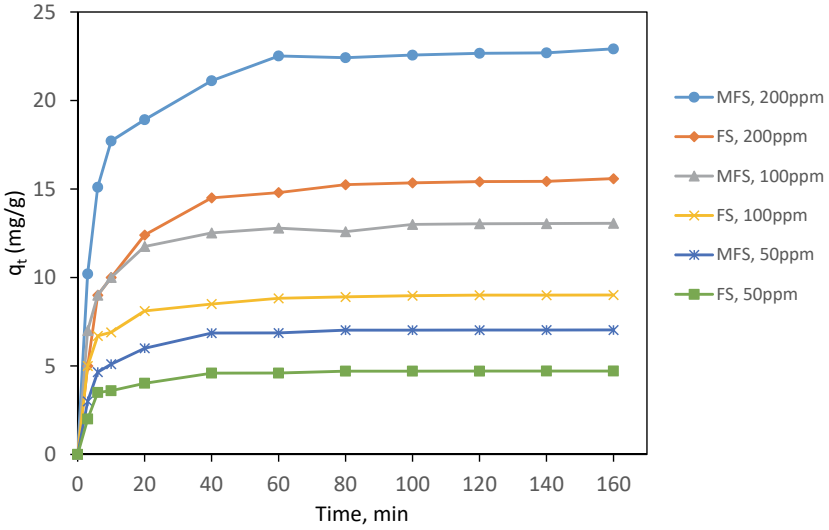

Fig. 9. The effect of contact time (kinetics of MB) onto the adsorption capacity of FS and MFS.

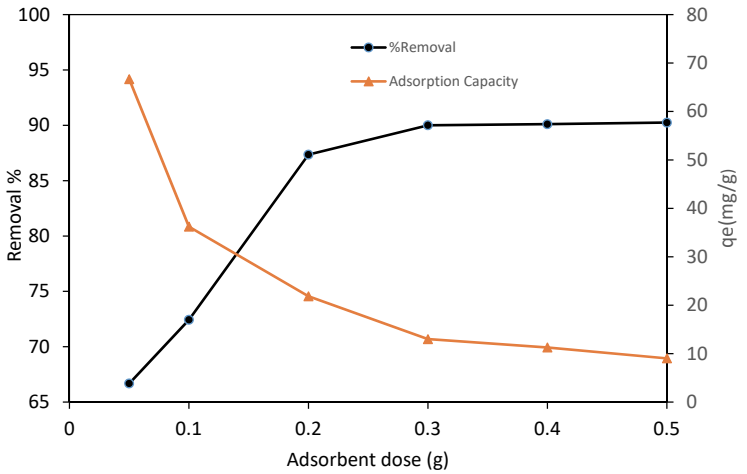

Fig. 10. The effect of adsorbent dosage on MB adsorption capacity and removal percentage.

molecules to the adsorbents and the equilibrium confirmation between MB bound to the adsorbent and those remaining unadsorbed in solution. As can be seen from Fig. 10, it is readily found that further increment in adsorbent dosage from 0.3 g did not cause significant improvement in removal percentage; therefore, this amount was selected as the optimum dosage for more experiments.

Adsorption Thermodynamics

The thermodynamic parameters of standard Gibbs free energy change (ΔG^0), standard entropy change (ΔS^0) and standard enthalpy change (ΔH^0) for the process of adsorption were estimated by the following equations [28]:

$$\Delta G^0 = -RTlnK_0 \quad (10)$$

$$lnK_0 = -\frac{\Delta H^0}{R}\frac{1}{T} + \frac{\Delta S^0}{R} \quad (11)$$

T, the absolute temperature in Kelvin and R is universal gas constant ($8.314 J/(mol.K)$). The thermodynamic distribution coefficient (K_0) for the process of adsorption can be obtained as following [29]:

$$K_0 = \frac{a_s}{a_e} = \frac{\upsilon_s}{\upsilon_e}\frac{C_s}{C_e} \quad (12)$$

Where, a_s and υ_s are, the activity and activity coefficient of the MB, respectively; and a_e and υ_e are, respectively, the activity and the activity coefficient of the MB in the equilibrium solution. C_s is the amount of MB adsorbed (mg) in every solvent liter in contact with the surface of the adsorbent. C_e is the amount of MB (mg) in every solvent liter in the equilibrium state. According to Biggar and Cheung [29], as the solute concentration in the solution approaches to zero, the coefficients of activity get the value equal to one, and therefore, Equation (12) can be defined as below:

$$\lim_{C_s \to 0} \frac{\upsilon_s}{\upsilon_e}\frac{C_s}{C_e} = \frac{C_s}{C_e} = \frac{a_s}{a_e} = K_0 \quad (13)$$

K_0 values can be estimated through plotting $ln(C_s/C_e)$ vs. C_s and extrapolating $C_s \to 0$. In the

Table 2. a) Thermodynamic parameters, b) Isotherm parameters, and c) Kinetic parameters

(a) Thermodynamic parameters		303 K	313 K	323 K
$\Delta G^0(Kj/mol)$		-7.3055	-6.1153	-5.2634
$\Delta H^0(Kj/mol)$				-38.299
$\Delta S^0(j/mol.K)$				-102.462
$E_a(kj/mol)$				-0.466
S^*				0.7555
(b) Isotherm models	Parameters	303 K	313 K	323 K
Langmuir	Q_{max} (mg/g)	58.47	64.21	68.72
	K_L (L/mg)	0.0367	0.0248	0.0191
	R^2	0.9935	0.995	0.99
Freundlich	n	2.592	2.262	2.075
	K_F $(mgg^{-1}(mgL^{-1})^{-1/n})$	7.298	5.595	4.578
	R^2	0.9534	0.9501	0.9375
Sips	Q_{max} (mg/g)	60.87	60.71	57.23
	$K_s((mg^{-1})^{-1/n})$	0.0419	0.0202	0.0078
	n	1.075	0.913	0.7361
	R^2	0.994	0.9958	0.9976
Redlich-Peterson	K_{RP} (Lkg^{-1})	2.42	1.504	1.082
	α $(kgmg^{-1})$	0.0571	0.0185	0.0045
	β	0.9391	1.044	1.233
	R^2	0.9941	0.9952	0.9933
(c) Kinetic models	Parameters	50 mg/L	100 mg/L	200 mg/L
Pseudo first	$q_{exp}(mg/g)$	7.03	13.06	22.92
order rate	$q_{cal}(mg/g)$	2.03	1.05	4.66
	k_1(1/min)	0.0329	0.0093	0.0249
	R^2	0.8353	0.7927	0.8685
Pseudo second	$q_{cal}(mg/g)$	7.08	13.16	23.42
order rate	k_2(g/mg.min)	0.1324	0.0473	0.0114
	R^2	0.9999	0.9997	0.9998

present study, thermodynamic parameters were obtained from the variation of the $\ln K_0$ vs. 1/T. The MB adsorption's thermodynamic parameters onto MFS are listed in Table 2a. The ΔG^0 negative values show that the process of adsorption is spontaneous and highly favorable at low temperatures. The $\Delta S°$ negative value reflects the decreased randomness at the interface of solid/solution in the process of adsorption [30].

The ΔH^0 value provides data about the effective forces on the process of adsorption. The energy is related to various physical forces including hydrophobic bond forces (5 kJ/mol), hydrogen bond forces (2–40 kJ/mol), van der Waals forces (4–10 kJ/mol), dipole bond forces (2–29 kJ/mol), coordination exchange (40 kJ/mol), and chemical forces (>60 kJ/mol) [30]. ΔH^0 was estimated equal to -38.299 kJ/mol, revealing that the physical forces including hydrogen bond forces and coordination exchange (in agreement with the results given in pH of point of zero charge section) affected the MB adsorption onto MFS. To confirm the fact that physical adsorption is the prominent mechanism, the sticking probability (S*) and activation energy (E_a) values were obtained from the data by employing an altered equation of Arrhenius type associated with the coverage of surface shown as following [31]:

$$S^* = (1-\theta)e^{-E_a/RT} \quad (14)$$

Sticking probability and energy of activation (Table 2a) were obtained from the intercept and slope of plot $Ln(1-\theta)$ versus 1/T with the reasonable good fit (data not shown, R^2>0.97); the surface coverage (θ) was calculated as below:

$$\theta = 1 - \frac{C}{C_0} \quad (15)$$

C_0 and C (mg/L) are, respectively, the initial and residual MB concentrations in the solution. The negative value of E_a indicates that the process of adsorption is basically exothermic. Relatively E_a low value proposes that adsorption is a diffusion controlled process. If 0<S*<1, then the adsorption process is physisorption. Eventually, according to the value of S^* (0.7555), the MB adsorption process onto MFS is physisorption.

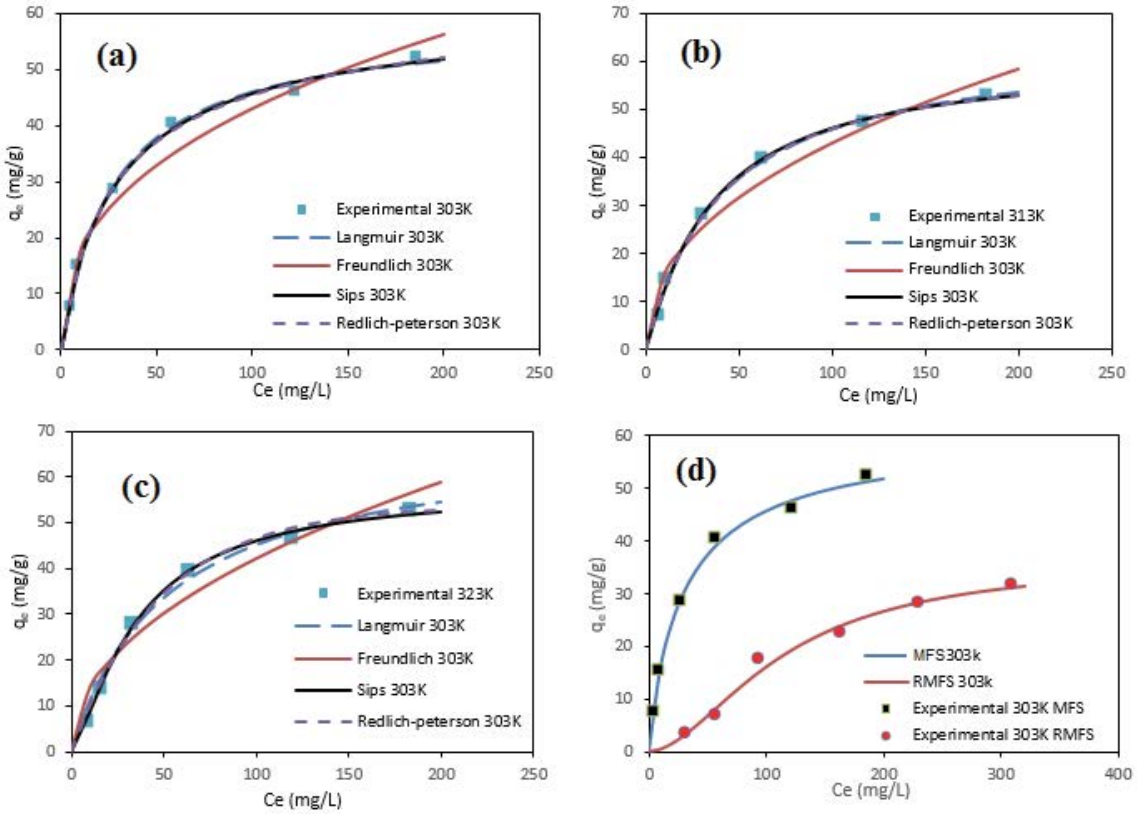

Fig. 11. Isotherm plots for MB adsorption onto MFS at (a) 303 K, (b) 313 K, (c) 323 K, and (d) Sips adsorption isotherm for MFS and RMFS at 303K.

Adsorption Isotherm Modeling

Fig. 11 and Table 2b represent the curves and fitting parameters of the calculated isotherms, respectively. The R^2 values for the Langmuir, Temkin, Sips, and Redlich-Peterson models show desired fitting with the data. Compared with other models the Freundlich model represented the poorest fitting with the experimental data at all temperatures ($0.93 < R^2 < 0.96$).

Fitting of isotherms can be expressed by the non-linear correlation coefficient (R^2), however, it seems that an acceptable correlation coefficient is not enough for a model to be expressed as a consistent model by which describes the adsorption process. The adsorption nature must also be considered to indicate an appropriate model. As thermodynamic analysis indicated (adsorption thermodynamics section), the adsorption of MB onto MFS is exothermic. So even though the Langmuir model shows acceptable fitting with the data ($R^2 < 0.99$), since the Langmuir maximum capacity of adsorption (Q_{max}) increases by increasing the temperature (Table 2b), it predicts the nature of the process inversely (endothermic). Since the Langmuir isotherm predicts adsorption for homogenous surfaces [18], thus the reason may be due to the heterogeneity of the adsorbent surface. On the other hand, the Sips model can achieve both a good fitting ($R^2 < 0.99$) and a correct prediction of the adsorption process nature (exothermic) simultaneously.

The Beta parameter (β) value in the Redlich-Peterson model is basically between zero and one [32]. When the value of β is equal to one, this equation become equalized to the Langmuir equation [33]. But in this study, the beta parameters of the Redlich-Peterson model were bigger than one (Table 2b). One possible explanation may be that $\beta > 1$ can confirm the deviation of the Langmuir model from the characteristic of the adsorption process. Based on Table 2b, as the β value gets bigger than one, the Langmuir model shows more deviation from the nature of process.

The Freundlich constant n renders a favorability of adsorption measure. n > 1values show a desired process of adsorption [31]. The value of n shows the same trend at all studied temperatures which shows the favorable nature characteristic of adsorption of MB by MFS. As it is clear from Table 2b, the value of n decreases by increasing the temperature; this confirms the adsorption's exothermic nature which is concluded formerly by thermodynamics analysis. According to the best correlation coefficient and the above explanations, Sips isotherm is the best model for describing the process of adsorption of MB onto MFS.

Adsorption Kinetics Studies

The linear forms of the rate of pseudo-first and pseudo-second-order equations were analyzed, and their parameters are represented in Table 2c. The adsorption kinetics of MB onto MFS is suggested to be successfully simulated by the pseudo-second-order kinetic model ($R^2 < 0.99$) in comparison with the pseudo-first-order kinetic model ($R^2 < 0.87$). The constant of pseudo-second-order rate declined from 0.1324 to 0.0114 g/mg.min by raising the initial dye concentration from 50 to 200 mg/L.

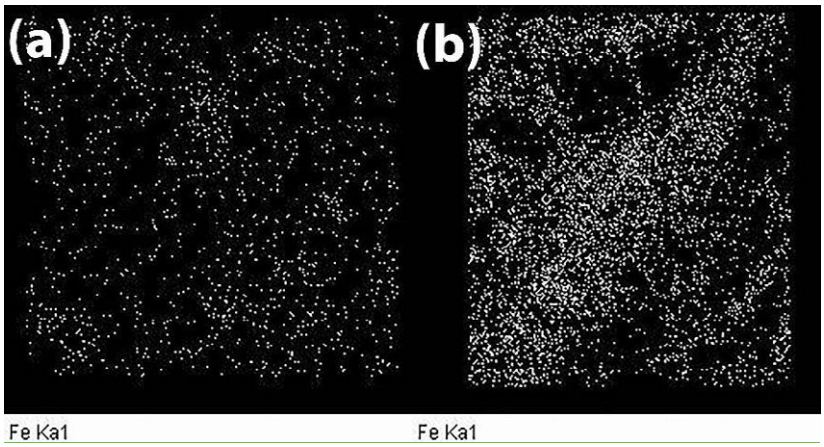

Fig. 12. Elemental mapping of Fe a) before regeneration process (UMFS), and b) after the regeneration process (RMFS).

Table 3. Comparison of the maximum adsorption capacity of various adsorbents

Adsorbent	Q_{max} (mg/g)	Reference
MFS	60.87	This work
RMFS	36.3	This work
Peanut hull	68.03	[8]
Walnut sawdust	59.17	[34]
Magnetic modified MWCNT	48.1	[35]
Rice husk	40.59	[36]
Nanomagnetic manganese oxide	35.4	[37]
Magnetic MWCNT	15.74	[38]
Fine grinded wheat straw	2.23	[39]

Regeneration Studies of the Adsorbent

The XRD patterns of adsorbent before and after the regeneration process is shown in Fig. 5c and d. The diffraction peaks at 2θ=26° and 32° were omitted after the regeneration process, which can be due to the extraction of minerals in FS by HCl. This conclusion can be approved by the EDX analysis (Table 1) where the atomic percent of all Na, Mg and Ca is almost equal to zero in RMFS.

Based on the EDX analysis, 75.19% of Fe was regenerated, which can approve the removal of MB from UMFS. The EDM analysis of Fe before and after regeneration of UMFS is shown in Fig. 12, where the white points represent Fe element. The increase of the atomic percent of Cl in RMFS (Table 1) is due to the regeneration of UMFS by HCl. The FESEM images before and after the regeneration process are shown in Fig. 3c and d.

It can be seen that that uniform layer of dye molecules in UMFS has been mostly cleared from the adsorbent surface, and the initial adsorbent's mesoporous structure has appeared. The equilibrium study was conducted for the regenerated adsorbent at 303 K. Since the Sips isotherm was concluded to be the best model predicting the adsorption of MB onto MFS, it was chosen for equilibrium analysis. A comparison of the MB adsorption isotherm to MFS and RMFS with Sips model is shown in Fig. 11d. The Sips maximum adsorption capacity (Q_{max}) was obtained as 36.3 mg/g for the RMFS adsorbent. The efficiency of the regeneration process can be defined as:

$$\text{Efficiency} = \frac{\text{The maximum adsorption capacity of RMFS}}{\text{The maximum adsorption capacity of MFS}} \quad (16)$$

So it can be concluded that the efficiency of the regeneration process at 303 K is equal to 59.63 %.

Comparison with Other Bioadsorbents

The comparison between MFS's maximum adsorption capacity (Q_{max}) and other low-cost adsorbents for MB adsorption is presented in Table 3. The results showed that both MFS and RMFS have an acceptable adsorption capacity compared to many other adsorbents, and can be suitable adsorbent candidates for water treatment.

CONCLUSION

The synthesis of a nano-magnetic FS was done by precipitation technique. The results showed a significant rise in the synthesized adsorbent's special surface area. The FS and MFS's specific surface areas were obtained, respectively, as 0.65 and 4.86 m^2/g. The analysis of SEM showed that the adsorbent was homogenized and smoothed, and had less porosity after the adsorption of MB. The EDX analysis revealed that the FS composition mainly included C, O, P and Ca elements. The isotherm results and negative ΔH^0 values suggest that the adsorption onto MFS is a physisorption process and exothermic in nature. The maximum adsorption capacity for the Sips model (best fitted isotherm) was 60.87 mg/g. The adsorption kinetics pursued the pseudo-second order kinetics model, and the regeneration process was achieved with the efficiency of 59.63%. Finally, an electrostatic interaction mechanism (among the negative groups on the MFS surface and positive groups of MB) was presented to explain the adsorption of MB onto MFS.

ACKNOWLEDGMENTS

The authors want to acknowledge from the University of Guilan and University of Tehran for the technical support.

CONFLICTS OF INTEREST

The authors declare that there are no conflicts of interest.

REFERENCES

1. Suárez L, Dong H, Pulgarin C, Sanjines R, Qiang Z, Kiwi J. Innovative photo-Fenton catalysis by PE-FeOx films leading to methylene blue (MB) degradation: Kinetics, surface properties and mechanism. Applied Catalysis A: General. 2016;519:68-77.
2. Johir MAH, Pradhan M, Loganathan P, Kandasamy J, Vigneswaran S. Phosphate adsorption from wastewater using zirconium (IV) hydroxide: Kinetics, thermodynamics and membrane filtration adsorption hybrid system studies. Journal of Environmental Management. 2016;167:167-74.
3. Zhao G-y, Liu L-j, Li J-r, Liu Q. Efficient removal of dye MB: Through the combined action of adsorption and photodegradation from NiFe 2 O 4 /Ag 3 PO 4. Journal of Alloys and Compounds. 2016;664:169-74.
4. Shakib F, Dadvand Koohi A, Kamran Pirzaman A. Adsorption of methylene blue by using novel chitosan-g-itaconic acid/bentonite nanocomposite – equilibrium and kinetic study. Water Science and Technology. 2017;75(8):1932-43.
5. Yagub MT, Sen TK, Afroze S, Ang HM. Dye and its removal from aqueous solution by adsorption: A review. Advances in Colloid and Interface Science. 2014;209:172-84.
6. Li D, Yan J, Liu Z, Liu Z. Adsorption kinetic studies for removal of methylene blue using activated carbon prepared from sugar beet pulp. International Journal of Environmental Science and Technology. 2016;13(7):1815-22.
7. Tizro S, Baseri H. Removal of Cobalt Ions from Contaminated Water Using Magnetite Based Nanocomposites: Effects of Various Parameters on the Removal Efficiency. Journal of Water and Environmental Nanotechnology. 2017;2(3):174-185.
8. Gong R, Ding Y, Li M, Yang C, Liu H, Sun Y. Utilization of powdered peanut hull as biosorbent for removal of anionic dyes from aqueous solution. Dyes and Pigments. 2005;64(3):187-92.
9. Ebrahimian Pirbazari A, Saberikhah E, Gholami Ahmad Gorabi N. Fe3O4nanoparticles loaded onto wheat straw: an efficient adsorbent for Basic Blue 9 adsorption from aqueous solution. Desalination and Water Treatment. 2014;57(9):4110-21.
10. Gupta VK, Suhas, Ali I, Saini VK. Removal of Rhodamine B, Fast Green, and Methylene Blue from Wastewater Using Red Mud, an Aluminum Industry Waste. Industrial & Engineering Chemistry Research. 2004;43(7):1740-7.
11. Ribeiro C, Scheufele FB, Espinoza-Quiñones FR, Módenes AN, da Silva MGC, Vieira MGA, et al. Characterization of Oreochromis niloticus fish scales and assessment of their potential on the adsorption of reactive blue 5G dye. Colloids and Surfaces A: Physicochemical and Engineering Aspects. 2015;482:693-701.
12. Zhu K, Gong X, He D, Li B, Ji D, Li P, et al. Adsorption of Ponceau 4R from aqueous solutions using alkali boiled Tilapia fish scales. RSC Advances. 2013;3(47):25221.
13. Muhammad N, Gao Y, Iqbal F, Ahmad P, Ge R, Nishan U, et al. Extraction of biocompatible hydroxyapatite from fish scales using novel approach of ionic liquid pretreatment. Separation and Purification Technology. 2016;161:129-35.
14. Chen S, Chen H, Xie Q, Hong B, Chen J, Hua F, et al. Rapid isolation of high purity pepsin-soluble type I collagen from scales of red drum fish (Sciaenops ocellatus). Food Hydrocolloids. 2016;52:468-77.
15. Huang C-Y, Kuo J-M, Wu S-J, Tsai H-T. Isolation and characterization of fish scale collagen from tilapia (Oreochromis sp.) by a novel extrusion–hydro-extraction process. Food Chemistry. 2016;190:997-1006.
16. Nadeem R, Ansari TM, Khalid AM. Fourier Transform Infrared Spectroscopic characterization and optimization of Pb(II) biosorption by fish (Labeo rohita) scales. Journal of Hazardous Materials. 2008;156(1-3):64-73.
17. Shi H, Li W, Zhong L, Xu C. Methylene Blue Adsorption from Aqueous Solution by Magnetic Cellulose/Graphene Oxide Composite: Equilibrium, Kinetics, and Thermodynamics. Industrial & Engineering Chemistry Research. 2014;53(3):1108-18.
18. Foo KY, Hameed BH. Insights into the modeling of adsorption isotherm systems. Chemical Engineering Journal. 2010;156(1):2-10.
19. Venkatesan G, Narayanan SL. Synthesis of Fe2O3-coated and HCl-treated bauxite ore waste for the adsorption of arsenic (III) from aqueous solution: Isotherm and kinetic models. Chemical Engineering Communications. 2017;205(1):34-46.
20. Huang Y-C, Hsiao P-C, Chai H-J. Hydroxyapatite extracted from fish scale: Effects on MG63 osteoblast-like cells. Ceramics International. 2011;37(6):1825-31.
21. Mota JA, Silva ES, Vieira EFS, Sussuchi EM, Cestari AR. A highly efficient adsorbent synthesized by reactive depositions of chitosan layers on fish scale collagen—Hydrodynamic swelling and dichlorophenol derivative sorption evaluated by continuous long-term solution microcalorimetry. Journal of Environmental Chemical Engineering. 2013;1(3):480-5.
22. Absalan F, Nikazar M. Application of Response Surface Methodology for Optimization of Water Treatment by Fe3O4/SiO2/TiO2Core-Shell Nano-Photocatalyst. Chemical Engineering Communications. 2016;203(11):1523-31.
23. Pashai Gatabi M, Milani Moghaddam H, Ghorbani M. Point of zero charge of maghemite decorated multiwalled carbon nanotubes fabricated by chemical precipitation method. Journal of Molecular Liquids. 2016;216:117-25.
24. Ho L-N, Ong S-A, Osman H, Chong F-M. Enhanced photocatalytic activity of fish scale loaded TiO2 composites under solar light irradiation. Journal of Environmental Sciences. 2012;24(6):1142-8.
25. Liu J, Cao J, Hu Y, Han Y, Zhou J. Adsorption of phosphate ions from aqueous solutions by a CeO 2 functionalized Fe 3 O 4 @SiO 2 core-shell magnetic nanomaterial. Water Science and Technology. 2017;76(11):2867-75.
26. Zhang F, Xu S, Wang Z. Pre-treatment optimization and properties of gelatin from freshwater fish scales. Food and Bioproducts Processing. 2011;89(3):185-93.
27. Cardoso NF, Lima EC, Pinto IS, Amavisca CV, Royer B, Pinto RB, et al. Application of cupuassu shell as biosorbent for the removal of textile dyes from aqueous solution. Journal of Environmental Management. 2011;92(4):1237-47.
28. Duan L, Hu N, Wang T, Wang H, Ling L, Sun Y, et al. Removal of Copper and Lead from Aqueous Solution by Adsorption onto Cross-Linked Chitosan/Montmorillonite Nanocomposites in the Presence of Hydroxyl–Aluminum Oligomeric Cations: Equilibrium, Kinetic, and Thermodynamic Studies. Chemical Engineering Communications. 2014;203(1):28-36.
29. Biggar JW, Cheung MW. Adsorption of Picloram (4-Amino-3,5,6-Trichloropicolinic Acid) on Panoche, Ephrata,

and Palouse Soils: A Thermodynamic Approach to the Adsorption Mechanism1. Soil Science Society of America Journal. 1973;37(6):863.
30. Kumar R, Barakat MA. Decolourization of hazardous brilliant green from aqueous solution using binary oxidized cactus fruit peel. Chemical Engineering Journal. 2013;226:377-83.
31. Ebrahimian Pirbazari A, Saberikhah E, Badrouh M, Emami MS. Alkali treated Foumanat tea waste as an efficient adsorbent for methylene blue adsorption from aqueous solution. Water Resources and Industry. 2014;6:64-80.
32. Wang S, Boyjoo Y, Choueib A, Zhu ZH. Removal of dyes from aqueous solution using fly ash and red mud. Water Research. 2005;39(1):129-38.
33. Liu Y, Liu Y-J. Biosorption isotherms, kinetics and thermodynamics. Separation and Purification Technology. 2008;61(3):229-42.
34. Ferrero F. Dye removal by low cost adsorbents: Hazelnut shells in comparison with wood sawdust. Journal of Hazardous Materials. 2007;142(1-2):144-52.
35. Madrakian T, Afkhami A, Ahmadi M, Bagheri H. Removal of some cationic dyes from aqueous solutions using magnetic-modified multi-walled carbon nanotubes. Journal of Hazardous Materials. 2011;196:109-14.
36. Vadivelan V, Kumar KV. Equilibrium, kinetics, mechanism, and process design for the sorption of methylene blue onto rice husk. Journal of Colloid and Interface Science. 2005;286(1):90-100.
37. Chen H, Chu PK, He J, Hu T, Yang M. Porous magnetic manganese oxide nanostructures: Synthesis and their application in water treatment. Journal of Colloid and Interface Science. 2011;359(1):68-74.
38. Gao H, Zhao S, Cheng X, Wang X, Zheng L. Removal of anionic azo dyes from aqueous solution using magnetic polymer multi-wall carbon nanotube nanocomposite as adsorbent. Chemical Engineering Journal. 2013;223:84-90.
39. Batzias F, Sidiras D, Schroeder E, Weber C. Simulation of dye adsorption on hydrolyzed wheat straw in batch and fixed-bed systems. Chemical Engineering Journal. 2009;148(2-3):459-72.